Bull. Mater. Sci. (2019) 42:8
https://doi.org/10.1007/s12034-018-1688-x

Effect of Nd doping on structural and opto-electronic properties of CdO thin films fabricated by a perfume atomizer spray method

M RAVIKUMAR[1], R CHANDRAMOHAN[2], K DEVA ARUN KUMAR[3], S VALANARASU[3,*], V GANESH[4], MOHD SHKIR[4], S ALFAIFY[4] and A KATHALINGAM[5]

[1]Department of Physics, Arumugam Pillai Seethai Ammal College, Tiruppattur 630211, India
[2]Department of Physics, Sree Sevugan Annamalai College, Devakottai 630303, India
[3]PG and Research Department of Physics, Arul Anandar College, Karumathur 625514, India
[4]Advanced Functional Materials & Optoelectronic Laboratory (AFMOL), Department of Physics, Faculty of Science, King Khalid University, Abha 61413, Saudi Arabia
[5]Millimeter-Wave Innovation Technology Research Center (MINT), Dongguk University-Seoul, Seoul 04620, Republic of Korea
*Author for correspondence (valanroyal@gmail.com)

MS received 30 October 2017; accepted 11 April 2018; published online 11 January 2019

Abstract. A perfume atomizer-assisted spray pyrolysis method was employed to fabricate undoped and neodymium (Nd)-doped cadmium oxide (CdO) thin films. X-ray diffraction results reveal that all the films are polycrystalline with a cubic structure with a preferential orientation along the (200) direction. Scherrer's formula was used to calculate the crystallite size of Nd-doped CdO films. Energy dispersive spectroscopy results show that Cd, Nd and O elements are present in Nd-doped CdO thin films. The optical absorption of the doped films is increased along with increasing Nd-doping level. The prepared CdO thin films have a high absorption coefficient in the visible region and the optical band gap is decreased on increasing Nd doping content. The electrical carrier concentration (n) of the deposited films is increased with increasing Nd doping concentration. Photoconductivity studies of a nanostructured Al/Nd–n-CdO/p-Si/Al device showed a non-linear electric characteristics indicating diode-like behaviour. Prepared Nd:CdO films could increase the photo-sensing effect of this n-CdO/p-Si heterostructure. These Nd-doped CdO thin films may open a new avenue for photodiode application in near future.

Keywords. Nd:CdO; spray using perfume atomizer; thin films; optical and electrical properties.

1. Introduction

Metal–oxide systems like zinc oxide (ZnO), cadmium oxide (CdO), tin oxide (SnO_2), titanium oxide (TiO_2), etc. have dual advantages associated with their electrical and optical properties that lead their applications to displays and light devices. These dual properties are high electrical conductivity and transparency. They are also suitable for applications like gas sensors, solar cells and a few other optoelectronic devices [1–6]. CdO shows high electrical conductivity due to the presence of oxygen vacancies. Electrical and optical properties of CdO can be modified by doping. Thin films of CdO were deposited using different techniques such as sol–gel [7], spray pyrolysis [8], magnetic sputtering [9], ion-beam sputtering [10], chemical vapour deposition [11], chemical-bath deposition [12] and pulsed-laser deposition [13]. Spray pyrolysis, which is one of the chemical techniques that are suitable to design thin films at a molecular level, has been applied to deposit a wide variety of thin films. The advantage of spray pyrolysis is its ability to be extended to large-scale fabrication. Also, morphology and structure can be modified easily by changing few parameters [14–17]. Recently, different rare-earth elements have been used as potential dopants in CdO structure and researchers are succeeded to explain the possibility of interaction and modification of various structural and physical properties of CdO films [18,19]. In view of this, in the present study from a series of rare-earth elements neodymium (Nd) has been chosen as a dopant element for CdO and the influence of Nd has been studied extensively on various properties like structural, electrical, optical and photo-conducting properties, and the results are discussed.

2. Experimental

Thin films of CdO with different concentrations of Nd doping were deposited onto heated glass substrates *viz.* a spray pyrolysis method using a perfume atomizer. Cadmium acetate (0.1 M) was mixed with deionized (DI) water with different weight % doping concentration of Nd (0, 1, 3 and 5%) and stirred for 10 min using a magnetic stirrer. This was

taken as the precursor. For the deposition, the prepared precursor is sprayed over a glass substrate. The glass substrate was pre-cleaned chemically with chromic acid and acetone, and then cleaned with DI water to remove contaminants, if any. The deposition parameters such as glass substrate temperature (350°C), spray time (10 s), interval (20 s), substrate to nozzle distance (30 cm) and spray angle (45°) are maintained constant for all growths. A temperature controller is used to maintain the temperature and monitored by the use of a thermocouple. The deposited film is allowed to cool to room temperature before taking to a sample box.

X-ray diffraction (XRD) patterns of the prepared Nd-doped CdO films were analysed by using an X-ray diffractometer (PANalytical) X'Pert PRO with Cu Kα radiation ($\lambda = 1.5418$ Å). The scan range of 2θ was set between 20 and 70° with a step of 0.02°. Micro-Raman spectra were recorded for the prepared thin films using a LABRAM-HR model with a He–Ne (632.8 nm) laser source. Fourier transform infrared (FTIR) spectra of the prepared samples were recorded using an FTIR (model: Bruker system) at room temperature under air condition with the wavenumber ranging between 400 and 4000 cm^{-1}. The surface morphology of the Nd-doped CdO thin films is characterized using scanning electron microscopy (SEM, Hitachi S-3000H). The optical transitions of the deposited films were determined using a UV-Vis-NIR double beam spectrometer (Perkin Elmer, Lambda 35). Emission properties were measured using a Horiba Jobin Yvon photoluminescence (PL) spectrometer. Electrical properties of the Nd-doped CdO films were analysed by Hall effect measurement by the use of a four-probe setup. The photocurrent of the device was recorded by using a Keithley 4200 semiconductor parameter analyser.

3. Results and discussion

3.1 *XRD analysis*

The XRD patterns of CdO thin films deposited at 350°C with different percentages of Nd doping (0, 1, 3 and 5%) are shown in figure 1. The observed peaks in the XRD pattern of the prepared films were appearing at (111), (200), (220) and (311) directions without any impurity and secondary phases. The obtained diffraction peaks in the XRD patterns are also in good agreement with the standard data for CdO (JCPDS data file no. 78-0653). The preferential orientation along the (200) plane observed here is in good agreement with reports on CdO thin films prepared by spray pyrolysis method [20]. From the XRD analysis, it is observed that all the prepared CdO thin films are polycrystalline in nature. The two major peaks (200) and (111) are observed for all the films. However, the strong intensity of the peak indicates the preferred orientation along the (002) plane with the *c*-axis perpendicular to the substrate of all the thin films. The (002) peak intensity was increased with increasing Nd doping concentrations is due to increasing crystalline nature of the prepared film.

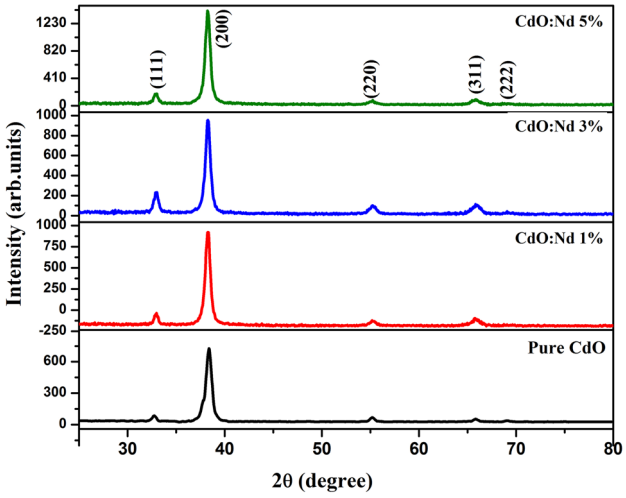

Figure 1. XRD patterns of undoped and Nd-doped CdO thin films.

A secondary (111) plane was observed for the films prepared with low Nd doping concentrations and it decreases for higher Nd doping concentration. This may be due to the evaporation of initial ingredients of precursor solution before reaching the substrate surface. The result shows that the crystallinity of the films increases with increasing Nd doping concentration. This may be due to increasing Nd doping content in the precursor solution, which promotes a coalescence process at the substrate that initiates an increase in the particle size as well as film thickness [21]. The observed lattice constant and structural parameters are presented in table 1. A few other parameters like texture coefficients (TC), microstrain (ε), number of crystallites per unit area (N) and dislocation density (δ) were estimated using usual relations.

Debye Scherrer's formula was used for calculation of crystallite size of CdO films as given in the following equation:

$$D = \frac{0.9\lambda}{\beta \cos\theta} \tag{1}$$

where λ, D, β and θ have usual meanings. Using the crystallite size values, the dislocation density and microstrain of the films were also determined using the below relations:

$$\delta = \frac{1}{D^2} \tag{2}$$

$$\varepsilon = \frac{\beta \cos\theta}{4}. \tag{3}$$

The crystallite size (D) varies from 15 to 21 nm for the Nd-doped CdO films. The fraction of layers undergoing faults in stacking sequence in a given crystal is called stacking fault probability and hence one fault is expected to be found in $1/\alpha$

Table 1. Thickness and structural parameters of Nd-doped CdO thin films.

CdO doped with Nd (%)	Thickness (nm)	Lattice const. (a) (Å)	Crystallite size (nm)	Dislocation density ($\delta \times 10^{15}$ lines m^{-2})	Strain ($\varepsilon \times 10^{-3}$ lines^{-2} m^{-4})	Stacking fault probability	No. of crystallites ($\times 10^{16}$)	Texture coefficient
0	600	4.6642	15	3.92	3.413	1.612	19	3.15
1	650	4.6851	16	3.91	2.026	1.601	19	3.25
3	730	4.6855	19	2.76	1.824	1.573	14	3.61
5	820	4.6850	21	2.18	1.621	1.421	10	3.76

layers. The relation between stacking fault probability and peak shift $\Delta(2\theta)$ is given by [22]

$$\alpha = \left[\frac{2\pi^2}{45\sqrt{3}}\right]\left[\frac{\Delta(2\theta)}{\tan\theta_{311}}\right]. \tag{4}$$

The stacking fault probability is a type of defect which characterizes the disorderness of the prepared CdO thin films. The stacking fault probability mainly depends on the position of peaks. The stacking fault probability value is low along the high crystallite size in doped CdO thin films.

The number of crystallites (N) per unit volume and dislocation density of different doping concentrations of CdO thin films were calculated using the following equation [23]:

$$N = \frac{t}{D^3}. \tag{5}$$

The number of crystallites per unit surface area and the dislocation density are found to be lower for the films coated at 5 wt% Nd. This result shows that the CdO thin film has a relatively higher crystalline quality compared with the other samples because the intensity of the (200) peak is high.

The TC was used to determine the preferred orientation by the following equation [24]:

$$\mathrm{TC}(hkl) = \frac{I(hkl)/I_0(hkl)}{N_r^{-1}\sum I(hkl)/I_0(hkl)}. \tag{6}$$

The calculated values of microstructural parameters such as D, δ, t, ε, TC and N of the (200) plane of the CdO thin films are presented in table 1. The TC represents the texture of a particular plane, deviation of which from unity implies the preferred growth. The value $\mathrm{TC}(hkl) < 1$ represents the lack of grains oriented in that direction [25]. Our observed TC value is greater than 1. The TC values significantly increases along with increasing Nd doping concentration due to increasing crystallinity.

3.2 *Vibrational analysis*

3.2a *Raman spectroscopy analysis*: Raman spectra of the CdO thin films were observed at room temperature in the region of 200–1200 cm^{-1}. The entire Raman spectrum for CdO film exhibits a relatively sharp structure at ~275 cm^{-1}, a broad structure covering the wavenumber ranging from 300 to 450 cm^{-1}, and a small peak at ~925 cm^{-1}. Similar data were obtained in previous Raman studies [26–28]. In principle, according to selection rules for the rocksalt structure both TO and LO modes are dipole forbidden; all features in the spectrum can be attributed to the second-order Raman scattering processes in CdO. The second-order Raman peaks observed are due to overtones and combination modes. All the Raman peaks for CdO shown in figure 2 can be attributed to its second-order Raman spectrum processes. Recently, two-phonon density of states (PDOS) calculations have identified a

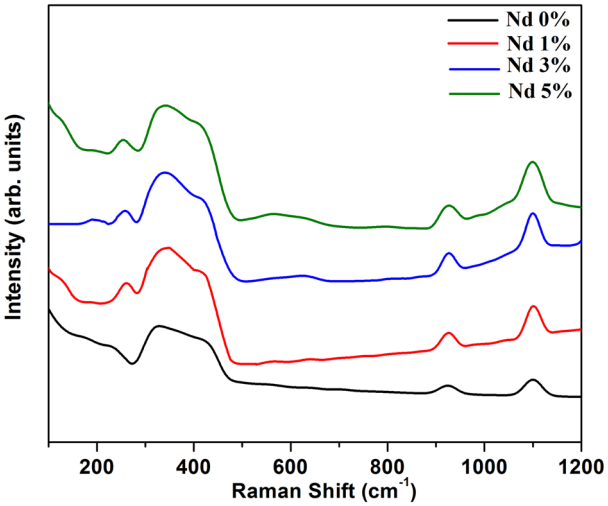

Figure 2. Raman spectra of undoped and Nd-doped CdO thin films.

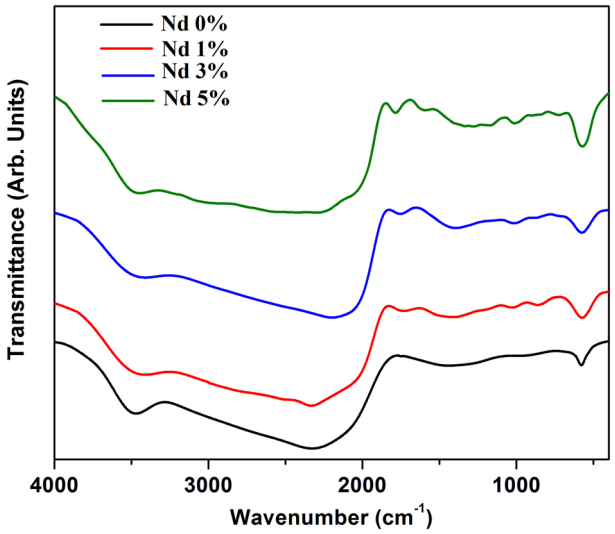

Figure 3. FTIR spectra of undoped and Nd-doped CdO films.

distinct peak at 275 cm^{-1} and TA and TO modes at the L-point of the Brillouin zone (BZ). The broad peak has been observed for CdO films around 300 cm^{-1} associated with phonon dispersion which is a signature of CdO that is assigned usually to 2TA(L) (transverse acoustic) mode. In the same studies, the multiple structures appearing between 300 and 450 cm^{-1} have been tentatively assigned to 2LA (longitudinal acoustic mode) overtones occurring at different high symmetric points of the BZ. A small peak at 925 cm^{-1} is appeared as the overtone of a 2LO occurring at the L- or C-point of the BZ. The peaks found near 935 and 1105 cm^{-1} are strong enough indicating the formation of nanostructures. A Raman shift around 945 cm^{-1} is assigned to 2LO. It is found that the intensity of the peak at 1100 cm^{-1} increases with increase in Nd concentration; these were associated with surface effects that induce longitudinal and transverse modes in the Raman spectrum [29].

3.2b *FTIR spectroscopy analysis*: The FTIR spectroscopy is the most common technique to identify the chemical bond structure. The FTIR spectra of the undoped and Nd-doped CdO films are shown in figure 3. The absorption peak at around 3400–3600 cm^{-1} is attributed to the normal polymeric O–H stretching vibration of H_2O in the CdO lattice. The sharp peak at 575 cm^{-1} confirmed the bonding of metal–oxygen (Cd–O) [30]. The observed peaks were confirmed the formation of a CdO thin film.

3.3 *SEM and energy dispersive X-ray spectroscopy analysis*

The surface morphology was analysed for all the films deposited with different Nd concentrations. Figure 4a–d shows the SEM images (unit scale is 2 μm) and microphotographs of Nd-doped CdO thin films. It is observed that the Nd-doped CdO thin films have uniform and homogeneous coverage of spherical grains. The undoped CdO film showed some holes with discontinuities on the film surface (figure 4a). Figure 4b–d indicates the voids and holes are slightly decreased with an increasing Nd doping level, which may be due to intrinsic stress caused by incorporation of foreign atoms [31]. Energy dispersive X-ray spectroscopy (EDX) is an analytical technique used for the chemical characterization of a sample. Figure 4e shows the EDX spectra of the prepared film at 5% Nd. The spectrum shows the presence of Cd, O and Nd elements in the deposited films. Figure 4e shows the presence of Cd, O and Nd as 48.1, 47.3 and 4.6%, respectively.

3.4 *Optical analysis*

Thickness is one the most important parameter for controls the film properties. The variation of film thickness with different Nd doping levels is presented in table 1. The observed film thickness is increased with increasing doping concentration due to the increasing interstitial position of Nd doping elements in the CdO lattice. Figure 5a shows the absorption spectra of the undoped and Nd-doped CdO thin films with various Nd doping contents. This study reveals that Nd-doped CdO film absorbs highly in the visible region, which is a characteristic of Nd-doped CdO. The absorbance in the UV-visible range increases with increasing Nd-doped content. The plot of optical transmittance *vs*. wavelength of CdO thin films deposited with spray pyrolysis with different wt% of Nd doping is shown in figure 5b. It is observed that all the deposited films exhibit transmittance ranging from 10 to 65% in the wavelength range of 480–1100 nm. The optical transmission is slightly decreased with the increase of Nd doping concentration which is noticed in the visible and near-infrared regions. The band gap of the deposited thin films

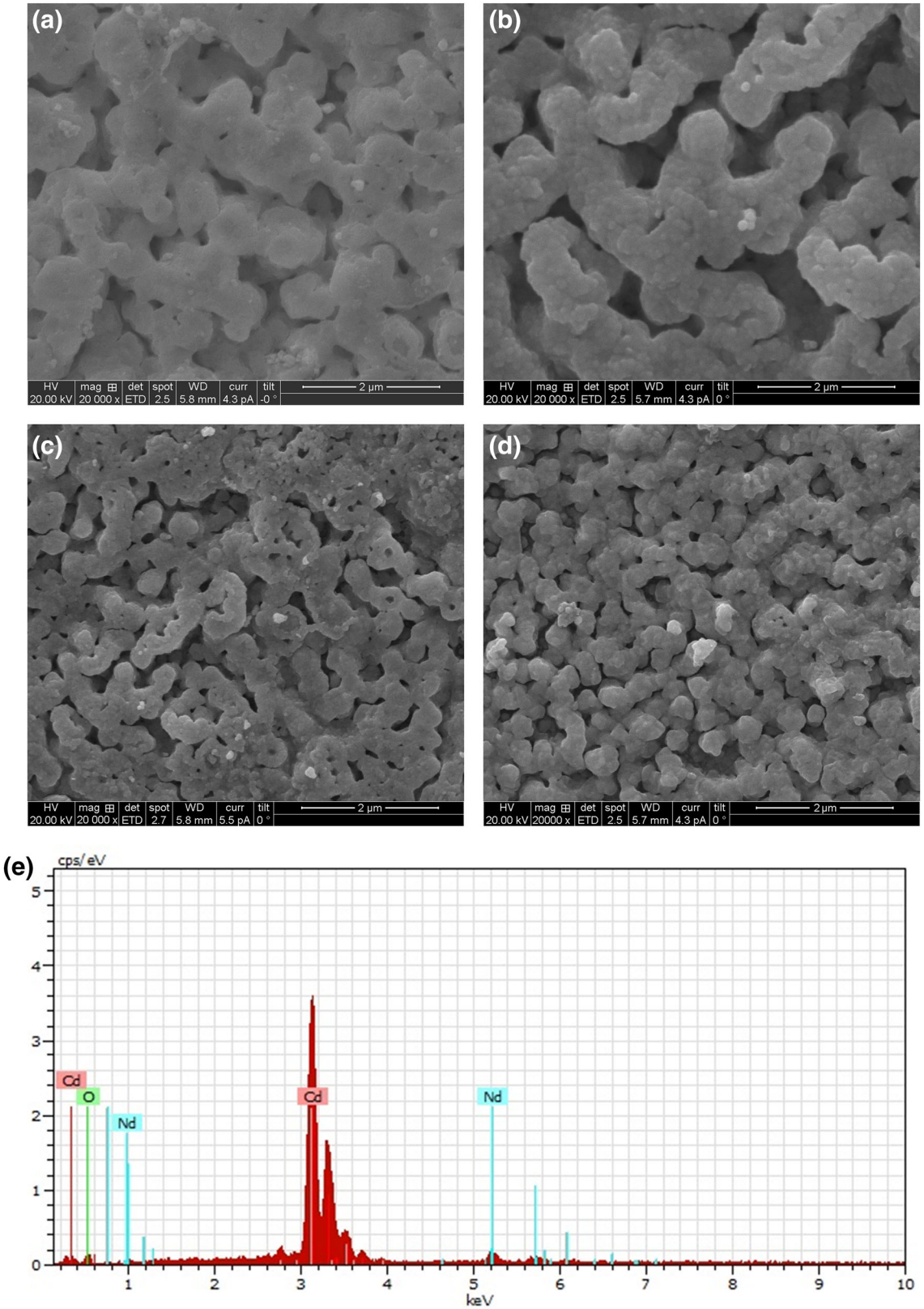

Figure 4. SEM micrographs of undoped and Nd-doped CdO: (**a**) pure, (**b**) 1%, (**c**) 3% and (**d**) 5% and (**e**) EDX spectrum of the 5% Nd-doped CdO thin film.

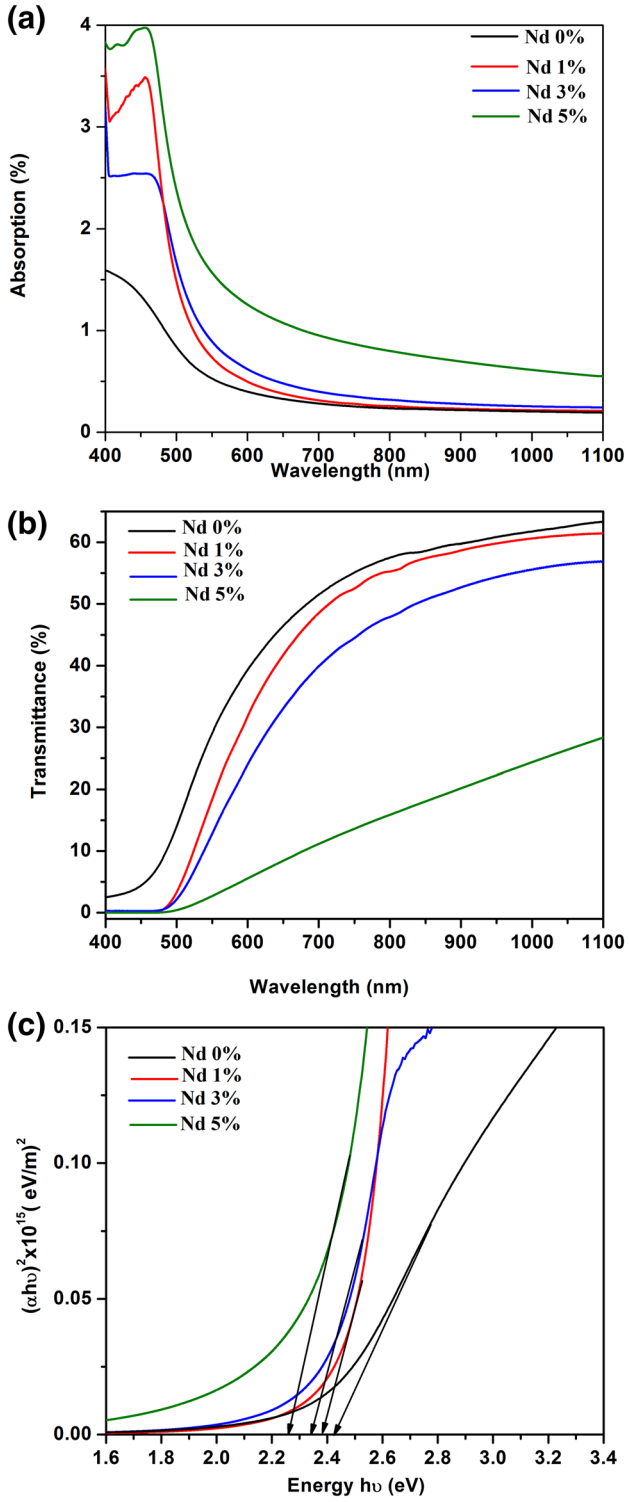

Figure 5. Plots of (**a**) absorbance, (**b**) transmittance and (**c**) band gap for 0%, 1%, 3% and 5 wt% Nd-doped CdO thin films.

can be obtained from the absorption coefficient (α) using equation (7) [32–34]:

$$\alpha = A(h\upsilon - E_g)^{n/2}. \quad (7)$$

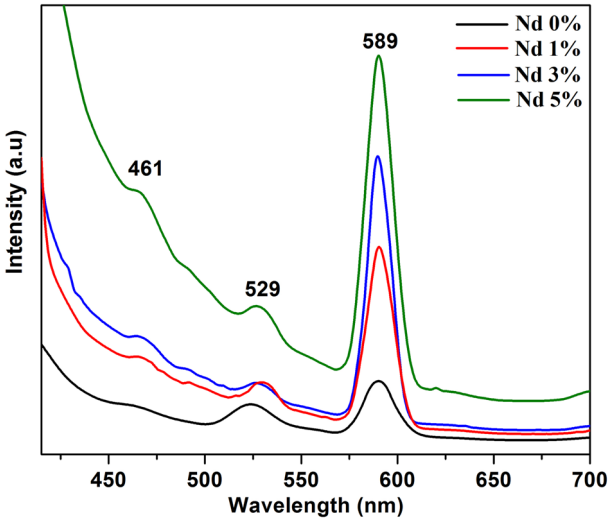

Figure 6. PL spectra of undoped and Nd-doped CdO thin films.

Figure 5c shows the band gap of the undoped and Nd-doped CdO films with various Nd contents. It is observed that the band gap values of CdO thin films vary from 2.42 to 2.25 eV with the effect of different % of Nd doping. The band gap of pristine CdO is in the range of 2.2–3.0 eV reported for the films prepared by different techniques [35–40] and near 2.2 eV reported for bulk CdO [41]. The decrease in the optical band gap of CdO with the increase in Nd doping concentration could be due to the structural modification in the CdO lattice which is due to the increase of either substitution or interstitial Nd^{3+} ions in the CdO lattice.

3.5 *Photoluminescence*

The spectra of photoluminescence (PL) were analysed at room temperature which reveal various peaks as shown in figure 6. PL spectroscopy can be used to determine the band gap of semiconductors. The most common radiative transition in the semiconductor occurs between states at the bottom of the conduction band and the top of the valence band. The PL spectra of the CdO thin films at room temperature with an excitation wavelength of 325 nm are shown in figure 6. The PL spectra show a sharp emission peak in the visible range centred at 589 nm and it may be due to the combination of electrons and holes from the conduction band and valance band [42]. The yellow emission was assigned to the oxygen vacancies and other defects in CdO and this luminescence resulted due to the recombination of photogenerated holes with ionized oxygen vacancies. The near band emission of the CdO thin films is observed at high intensity peak which is due to the radioactive recombination of electrons and holes from the conduction band and valance band [43]. The PL intensity of green emission around 461 nm increases with increasing [Nd]/[Cd] ratio. The green emissions were arising due to the presence of an excess of free electrons and point defects as V_O. Once again this may be associated with the increase of thermal energy and

oxidation [44]. The observed peak at 529 nm may be due to the deep trap emission and surface-state emission usually are independent of size of the traps [45]. PL peak positions have previously been reported [39]. The peak at 528 nm is surface state emission which is also independent of size. The quantum confinement changes the MBE emission as reported [46].

3.6 *Electrical analysis*

At room temperature, Hall Effect measurements were performed in a van der Pauw configuration. The type of conduction is confirmed to be n-type by the negative sign of Hall coefficient. Figure 7 illustrates the variation in resistivity (ρ), carrier concentrations (n) and Hall mobility (μ) as a function of Nd concentration in CdO thin films and these values are listed in table 2. It can be seen that the electrical parameters were strongly influenced by doping in the CdO films. The carrier concentration (n) was increased by increasing the Nd doping % concentration. The lower resistivity (ρ) (0.552×10^{-3} Ω cm) and higher carrier concentration (6.165×10^{20} cm^{-3}) are observed for 5% Nd concentration. Resistivity (ρ) for different Nd doping is 0.835×10^{-3}, 0.820×10^{-3}, 0.665×10^{-3} and 0.552×10^{-3} Ω cm, carrier concentration (n) is 3.547×10^{20}, 4.448×10^{20}, 5.369×10^{20} and 6.165×10^{20} cm^{-3} and carrier mobility (μ) is 21.11, 16.51, 17.51 and 18.36 $cm^2\,V^{-1}\,s^{-1}$, respectively.

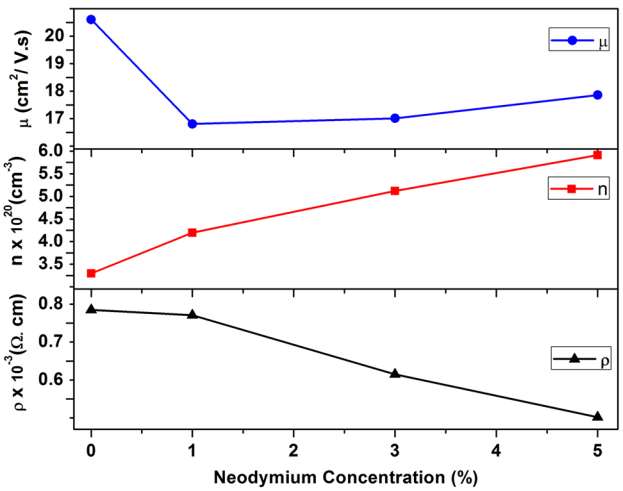

Figure 7. Carrier concentration (n), hall mobility (μ) and resistivity (ρ) plots of undoped and Nd-doped CdO thin films.

The observed electrical resistivity of the Nd-doped CdO is in good agreement with CdO thin films by spray pyrolysis [42]. As is well known, the resistivity is proportional to the reciprocal of the product of carrier concentration and mobility. The improvement in electrical properties may be due to improved carrier concentration. From the Hall measurement data, it is evident that the increase of % Nd doping causes a decrease in electrical resistivity.

3.7 *Photo-analysis*

The photo-response study of the Nd-doped CdO thin films was carried out using a 200 W halogen lamp as a photoexcitation source. Figure 8 shows the Al/Nd–n-CdO/p-Si/Al heterojunction of the 5% Nd-doped CdO thin film. Figure 9 shows the I–V characteristics of an Nd-doped CdO thin film diode in the forward and reverse directions under dark and illumination conditions. It is clear that the diode exhibited an illumination sensitive behaviour. It was found that the reverse current increases under illumination conditions for a given reverse voltage and is higher than the dark current. This indicates that the diode exhibits a photodiode behaviour.

The current through a Schottky diode according to thermionic emission (TE) theory is given by [47]

$$I = I_0 \exp\left(\frac{qV}{nKT} - 1\right). \tag{8}$$

In the above equation, q is the electron charge, I_0 is the reverse saturation current, V is the applied voltage, n is the ideality factor, K is the Boltzmann constant and T is the absolute temperature. The diode ideality factor (n) and the reverse bias saturation current (I_0) are determined from the slope and the intercept of a semi-logarithmic forward bias I–V plot for $V > 3kT/q$ using equation (8) and n and ϕ_b are given by [48]

$$n = \frac{q}{KT}\frac{dV}{d(\ln I)} \tag{9}$$

$$\phi_b = \frac{KT}{q}\ln\left(AA^*T^2/I_0\right), \tag{10}$$

where A is the effective diode area and A^* is the effective Richardson constant. The mechanism of transportation in the thin film, associated with the changes in the transport phenomenon, is understood by analysing I–V characteristics. The I–V characteristics of a typical p-Si/n-CdO device

Table 2. Electrical values of Nd-doped CdO.

CdO doped with Nd (%)	Resistivity (Ω cm)	Carrier concentration (cm^{-3})	Carrier mobility (μ) ($cm^2\,V^{-1}s^{-1}$)
0	0.835×10^{-3}	3.547×10^{20}	21.11
1	0.820×10^{-3}	4.448×10^{20}	16.51
3	0.665×10^{-3}	5.369×10^{20}	17.51
5	0.552×10^{-3}	6.165×10^{20}	18.36

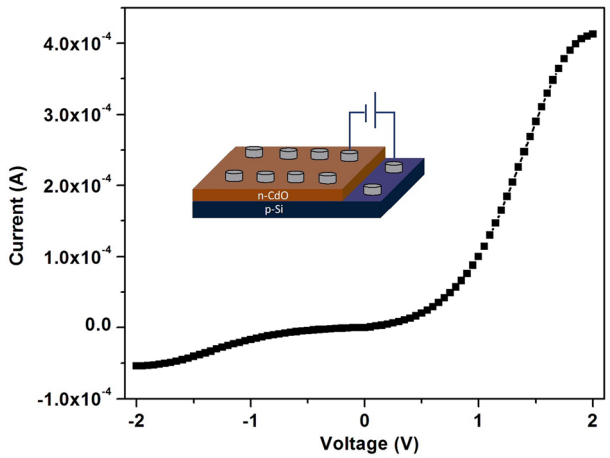

Figure 8. I–V characteristic of the 5% Nd-doped CdO/Si heterostructure.

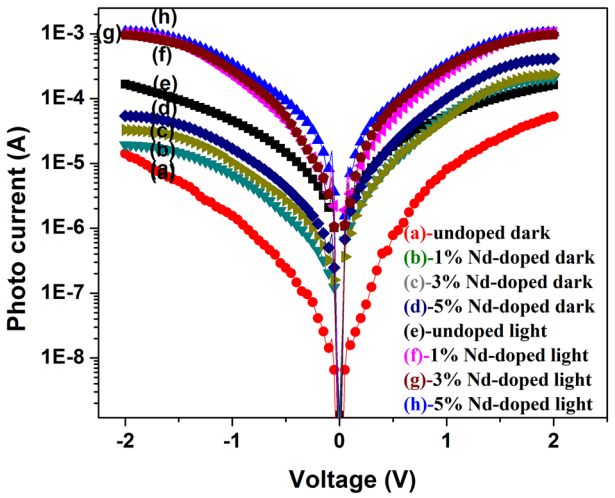

Figure 9. Forward and reverse I–V characteristics of the devices under dark and illumination for Nd-doped and undoped CdO thin films.

are given. The current is measured from zero bias voltage to positive side up to 2 V. The applied voltage is slowly decreased until zero both in forward and reversed biases. In the fabricated heterojunction diode, the turn-on voltage is observed as 0.86 V. The turn-on voltage, also identified as the diffusion or built-in potential, would correspond to a potential barrier such that charged carriers across the barrier contribute to forward current [49]. It shows positive response to light due to the large amount of electrons emitted from the excitation state with high-surface energy. The semi-logarithmic I–V curve of the device is constructed. The ideality factor is calculated from the slope of the linear region of the forward bias ln I–V curves and found to be 4.05 using equation (9). The ideality factor obtained at room temperature for the p-Si/n-CdO heterojunction was found to be −2 V. The above values are in good agreement with the previous results of CdO doped with Gd [50]. For an ideal diode, the ideality factor is unity but in this case, the higher value of n may be due to the interface states, non-uniformity of the CdO deposited film, series resistance or an interfacial layer between the p-Si and n-CdO films. The reverse saturation current I_0 is determined from the y-intercept of the semi-logarithmic curve and its value is 1.8088×10^{-6} A. Using equation (10), the value of ϕ_b is calculated as 0.61 eV for the 5% Nd-doped CdO film. The photocurrent increases up to a certain level after illumination. As the illumination turns on the number of free charge carriers increases and the current may be due to the photogenerated electrons. This result confirms the photoconductivity behaviour of the fabricated device. The following relation expresses the responsivity (R) of the diode [51]:

$$R = \frac{I_{ph}}{PA}. \tag{11}$$

In the above equation, I_{ph} is the photocurrent, P is the irradiation of the lamp and A is the effective area of the diode. The value of the photoresponsivity (R) of the Al/Nd–n-CdO/p-Si/Al hybrid heterojunction diode is found to be 343 mA W^{-1} at a bias of −2 V. Nd-doped CdO could increase the photo-sensing effect of this n-CdO/p-Si heterostructure. This increase may be due to the decrease of the energy gap value, the improved crystalline quality of the films and grain size. The calculated photodiode values are presented in table 3.

4. Conclusion

Nd-doped CdO thin films have been successfully deposited onto glass and silicon substrates using a simple perfume atomizer technique. In our experiment, XRD study shows the

Table 3. Photoresponse study of the Nd-doped CdO.

CdO doped with Nd (%)	Potential barrier (ϕ_b) (eV)	Ideality factor (n)	Photoresponsivity (R) (mA W^{-1})	Quantum efficiency (η) (%)
0	0.73	4.57	182	38.82
1	0.70	4.41	243	51.03
3	0.69	4.36	328	68.88
5	0.61	4.05	343	73.03

formation of pure CdO thin films with a cubic structure. The optical band gap values are in the range of 2.42–2.25 eV. The morphology of the deposited films has been found to be smooth and nearly spherical grains that consist of clusters formed with the nanoparticles. From FTIR studies, the strong peak of the Cd–O stretching mode was observed at 575 cm^{-1} . The electrical studies showed the film has a lower resistivity of $0.552 \times 10^{-3}\ \Omega\,cm$, and higher carrier concentration $6.165 \times 10^{20}\ cm^{-3}$ for 5 wt% Nd. We have fabricated an Al/Nd–n-CdO/p-Si/Al heterojunction diode with a photoresponsivity of 343 mA W^{-1}. The obtained results show that the Al/Nd–n-CdO/p-Si/Al heterojunction diode can be used for photosensors and other optoelectronic applications.

Acknowledgements

We would like to express our gratitude to King Khalid University, Saudi Arabia for providing administrative and technical support.

References

[1] Ito N, Sato Y, Song P K, Kaijio A, Inoue K and Shigesato Y 2006 *Thin Solid Films* **496** 99
[2] Lim J T, Jeong C H, Vozny A, Lee J H, Kim M S and Yeom G Y 2007 *Surf. Coat. Technol.* **201** 5358
[3] Navamathavan R, Choi C K and Park S J 2009 *J. Alloys Compd.* **475** 889
[4] Ilican S, Caglar Y, Caglar M, Kundakci M and Ates A 2009 *Int. J. Hydrog. Energy* **34** 5201
[5] Deva Arun Kumar K, Valanarasu S, Jeyadheepan K, Hyun-Seok K and Dhanasekaran V 2018 *J. Mater. Sci.: Mater. Electron.* **29** 3648
[6] Deva Arun Kumar K, Ganesh V, Shkir M, Alfalfa S and Valanarasu V 2018 *J. Mater. Sci. Mater. Electron.* **29** 887
[7] Cruz J S, Delgado G T, Perez R C, Romero C I Z and Angel O Z 2007 *Thin Solid Films* **515** 5381
[8] Vigil O, Cruz F, Morales-Acevedo A, Contreras-puente G, Vaillant L and Santana G 2001 *Mater. Chem. Phys.* **68** 249
[9] Subramanyam T K, Uthanna S and Naidu B S 1998 *Mater. Lett.* **35** 214
[10] Chu T L and Chu S S 1963 *J. Electrochem. Soc.* **110** 548
[11] Zhao Z, Morel D L and Ferekides C S 2002 *Thin Solid Films* **413** 203
[12] Gutierrez L R L, Romero J J C, Tapia J M P, Calva E B, Flores J C M and Lopez M O 2006 *Mater. Lett.* **60** 3866
[13] Gupta R K, Ghosh K, Patel R, Mishra S R and Kahol P K 2008 *Mater. Lett.* **62** 4103
[14] Yagi I, Hagiwara Y, Murakami K and Kaneko S 1993 *J. Mater. Res.* **81** 481
[15] Joseph Edison D, Nirmala W, Deva Arun Kumar K, Valanarasu S, Ganesh V, Shkir M *et al* 2017 *Physica B* **523** 31
[16] Murakami K, Yagi I and Kaneko S 1996 *J. Am. Ceram. Soc.* **79** 2557
[17] Kaneko S, Yagi I, Kosugi T and Murakami K 1998 in: A P Tomsia and A M Glaeser (eds) *Ceramic microstructures* (Boston, MA: Springer)
[18] Gupta R K, Ghosh K, Patel R and Kahol P K 2011 *J. Alloys Compd.* **509** 4146
[19] Gupta R K, Serbetci Z and Yakuphanoglu F 2012 *J. Alloys Compd.* **515** 96
[20] Deokate R J, Pawar S M, Moholkar A V, Sawant V S, Pawar C A, Bhosale C H *et al* 2008 *Appl. Surf. Sci.* **254** 2187
[21] Herednis D P and Gauckler L J 2005 *J. Electroceram.* **14** 103
[22] Mariappan R, Ragavendar M and Ponnuswamy V 2011 *J. Alloys Compd.* **509** 7337
[23] Shkir M, Ganesh V, AlFaify S, Yahia I S and Zahran H Y 2018 *J. Mater. Sci.: Mater. Electron.* **29** 6446
[24] Valanarasu S, Dhanasekaran V, Karunakaran M, Vijayan T A, Chandramohan R and Maalingam T 2014 *J. Mater. Sci.: Mater. Electron.* **25** 3846
[25] Deva Arun Kumar K, Valanarasu S, Tamilnayagam V and Amalraj L 2017 *J. Mater. Sci.: Mater. Electron.* **28** 14209
[26] Cusco R, Ibanez J, Domenech-Amador N, Artus L, Zuniga-Perez J and Munoz Sanjose V 2010 *J. Appl. Phys.* **107** 063519
[27] Oliva R, Ibanez J, Artus L, Cusco R, Zuniga-Perez J and Muno Sanjose V 2013 *J. Appl. Phys.* **113** 053514
[28] Sahin B 2013 *Sci. World J.* **2013** 1
[29] Thema F T, Beukes P, Gurib-Fakim A and Maaza M 2015 *J. Alloys Compd.* **646** 1043
[30] Knaepen E, Mullens J, Yperman J and Poucke L C V 1996 *Thermochim. Acta* **284** 213
[31] Thirumoorthi M and Thomas J P 2015 *J. Asian Ceram. Soc.* **4** 39
[32] Shkir M and AlFaify S 2017 *Sci. Rep.* **7** 16091
[33] Shkir M, Ganesh V, AlFaify S and Yahia I S 2017 *J. Mater. Sci.: Mater. Electron.* **28** 10573
[34] Shkir M, Yahia I S, Ganesh V, Algarni H and AlFaify S 2016 *Mater. Lett.* **176** 135
[35] Dakhel A A 2009 *J. Alloys Compd.* **475** 51
[36] Ravikumar M, Ganesh V, Shkir M, Chandramohan R, Deva Arun Kumar K, Valanarasu S *et al* 2018 *J. Mol. Struct.* **1160** 311
[37] Dakhel A A 2009 *Sol. Energy* **83** 934
[38] Kawamura K, Maekawa K, Yanagi H, Hirano M and Hosono H 2003 *Thin Solid Films* **445** 182
[39] Ueda N, Maeda H, Hosono H and Kawazoe H 1998 *J. Appl. Phys.* **84** 6174
[40] Xu Y and Schoonen M A A 2000 *Am. Mineral.* **85** 543
[41] Nese K, Sertap Kavasoglu A and Sener O 2009 *J. Phys. Chem. Solids* **70** 521
[42] Sankarasubramanian K, Soundarrajan P, Sethuraman K, Ramesh Babu R and Ramamurthi K 2014 *Superlattices Microstruct.* **69** 29
[43] Sui Y R, Cao Y, Li X F, Yue Y G, Yao B, Li X Y *et al* 2015 *Ceram. Int.* **41** 587
[44] Dingle R 1969 *Phys. Rev. Lett.* **23** 579
[45] Dong W and Zhu C 2003 *Opt. Mater.* **22** 227
[46] Jun Kuo T, Micheal Z and Huang H 2006 *J. Phys. Chem. B* **110** 13717
[47] Rhoderick E H and Williams R H 1988 *Metal-semiconductor contacts* 2nd edn (Oxford: Clarendon)

[48] Ugurel S A E, Serifoglu K and Turut A 2008 *Microelectron. Eng.* **85** 2299
[49] Chen P, Ma X and Yang D 2007 *J. Appl. Phys.* **101** 053103
[50] Ravikumar M, Chandramohan R, Deva Arun Kumar K and Valanarasu S 2018 *J. Sol-Gel Sci. Technol.* **85** 31
[51] Naderi N and Hashim M R 2013 *J. Alloys Compd.* **552** 356